

N-body chaos and the continuum limit in numerical simulations of self-gravitating systems, revisited

Pierfrancesco Di Cintio^{1,2*} and Lapo Casetti^{2,3,4}

¹ *Consiglio Nazionale delle Ricerche, Istituto di Fisica Applicata “Nello Carrara”, via Madonna del piano 10, I-50019 Sesto Fiorentino, Italy*

² *INFN - Sezione di Firenze, via G. Sansone 1, I-50019 Sesto Fiorentino, Italy*

³ *Dipartimento di Fisica e Astronomia and CSDC, Università di Firenze, via G. Sansone 1, I-50019 Sesto Fiorentino, Italy*

⁴ *INAF - Osservatorio Astrofisico di Arcetri, largo Enrico Fermi 5, I-50125 Firenze, Italy*

Accepted... Received...; in original form...

ABSTRACT

We revise the rôle of discreteness and chaos in the dynamics of self-gravitating systems by means of *N*-body simulations with active and frozen potentials, starting from spherically symmetric stationary states and considering the orbits of single particles as well as the orbits of the system in the full $2N$ -dimensional phase space. We investigate the dependence on *N* of the largest Lyapunov exponent both of single particle orbits and of the full *N*-body system. We also show that the use of frozen *N*-body potentials may be misleading in certain cases.

Key words: Chaos – gravitation – galaxies: evolution – methods: numerical

1 INTRODUCTION

The dynamics of *N*-body self-gravitating systems, due to the long-range nature of the $1/r^2$ force, is dominated by mean field effects rather than by inter-particle collisions, for sufficiently large particle number *N*. It is then natural to adopt a description in the continuum and collisionless limit $N \rightarrow \infty$, with $m \rightarrow 0$, where *m* is the individual particles’ mass. The system is described by the single-particle distribution function $f(\mathbf{r}, \mathbf{v}, t)$ in phase space, where \mathbf{r} is the position and \mathbf{v} is the velocity, and the time evolution of f is dictated by the collisionless Boltzmann-Poisson equations (CBE, see e.g. Binney & Tremaine 2008)

$$\begin{cases} \partial_t f + \mathbf{v} \cdot \nabla_{\mathbf{r}} f + \nabla \Phi \cdot \nabla_{\mathbf{v}} f = 0 \\ \Delta \Phi(\mathbf{r}) = -4\pi G \rho(\mathbf{r}) = -4\pi G \int f \, d\mathbf{v}, \end{cases} \quad (1)$$

linking f to the (in principle time-dependent) density-potential pair (ρ, Φ) ; G is the gravitational constant. Equations (1) yield a faithful description of the dynamics as long as the effect of binary encounters on the time evolution of f may be neglected: this happens for times shorter than the two-body relaxation time t_{2b} . The relevant fact (holding true for any long-range-interacting system, not only for self-gravitating ones; see e.g. Campa et al. 2014, 2009) is that such a timescale grows with *N*. In the case of self-gravitating systems the relaxation time may be estimated as

(Chandrasekhar 1941; Binney & Tremaine 2008)

$$t_{2b} = \frac{v_{\text{typ}}^3}{8\pi(Gm)^2 n \ln \Lambda} \approx \frac{N}{8 \ln N} t_{\text{dyn}}, \quad (2)$$

where $t_{\text{dyn}} = r_c/v_{\text{typ}}$, with r_c and v_{typ} the typical size and velocity scale of the system, n is an average number density and $\ln \Lambda$ is the so-called Coulomb logarithm, i.e., the logarithm of the ratio of the maximum to minimum impact parameter between the system’s particles, typically a number of order 10. Therefore, large *N* systems such as elliptical galaxies, where $N \approx 10^{11}$, have two-body relaxation times far exceeding the Hubble time, so that discreteness effects and dynamical collisions can be safely neglected, assuming Eqs. (1) valid over all physically relevant times.

However, self-gravitating systems are often studied by means of *N*-body simulations, numerically integrating the equations of motion of a system of *N* particles interacting via gravitational forces. First of all, we note that the in a numerical simulation the number of particles is much smaller than the real number of stars in a galaxy. As a consequence, the relaxation time t_{2b} , measured in units of the dynamical time t_{dyn} , is orders of magnitudes smaller than the relaxation time of the system one would like to simulate¹. Therefore, a direct numerical simulation of a collisionless system might be con-

¹ For instance, consider a galaxy of 10^{11} solar masses for which $t_{\text{dyn}} \approx 10^8$ yrs and $t_{2b} \approx 10^{16}$ yrs. A numerical simulation using 10^9 particles will have a smaller t_{2b} , roughly of a factor 10^{-6} !

* E-mail: p.dicintio@ifac.cnr.it

sidered² “truly collisionless” only for sufficiently small times. Moreover, a gravitational N -body system is a chaotic dynamical system. Since the pioneering work by Miller (1964, 1971) (see also Hemsendorf & Merritt 2002; Helmi & Gomez 2007), an apparent contradiction has shown up: on the one hand, when increasing the number of particles of a model, while keeping for example the total mass fixed, the sensitivity to the initial conditions (i.e., dynamical chaos) should increase, while on the other hand, its continuum limit represented by Eqs. (1) is a non-canonical infinite-dimensional Hamiltonian system that admits an infinite number of conserved quantities (the so-called Casimir invariants, or casimirs, Kandrup 1998a) and one would expect the systems to become less chaotic when getting closer to the continuum limit, i.e., by increasing N .

All these observations led to question the validity of the continuum limit, at least from the point of view of numerical simulations and their interpretation (see e.g. Kandrup 1998b; El-Zant et al. 2018). For example, in a series of papers, Kandrup and collaborators investigated the validity of such limit and the effect of discreteness noise using single particle orbit analysis in frozen N -body models (Kandrup & Sideris 2001; Sideris & Kandrup 2002; Sideris 2002; Kandrup & Sideris 2003; Kandrup et al. 2004; Sideris 2004), and Langevin-like stochastic equations (Kandrup 2001; Kandrup et al. 2003; Terzić & Kandrup 2003; Kandrup & Siopis 2003; Kandrup & Novotny 2004; Sideris & Kandrup 2004). Moreover, Hemsendorf & Merritt (2002) explored the linear stability of self-consistent equilibrium N -body systems as a function of N , finding a logarithmic growth rate of the perturbation with the particle number. Dynamical chaos, i.e., the exponential sensitivity to the initial conditions, is customarily measured by the largest Lyapunov exponent λ_{\max} (see e.g. Lichtenberg & Lieberman (1992) and the discussion in Sec. 2.2 below). In the context of one-dimensional gravity, Tsuchiya & Gouda (2000a,b) investigated the dependence of λ_{\max} on N finding a curious $\lambda_{\max} \propto N^{-1/5}$ scaling. Manos & Ruffo (2011) and Ginelli et al. (2011) repeated the analysis of the behaviour of λ_{\max} with N for another long-range-interacting one-dimensional system, the so-called Hamiltonian Mean-Field model (HMF, Antoni & Ruffo 1995) and its two-dimensional generalization. These studies suggest a scaling of the form $\lambda_{\max} \propto N^{-1/3}$ or $\lambda_{\max} \propto 1/\ln N$, depending on the total energy³ of the model in the finite N regime; these results have been confirmed by Filho et al. (2018). Similar scalings of λ_{\max} with N were found by Monечи & Casetti (2012) for the self-gravitating ring model, where particles interacting via softened gravitational forces are constrained on a ring. The study of chaotic dynamics and Lyapunov exponents in full N -body self-gravitating systems in three dimensions has been carried out by Cerruti-Sola & Pettini (1995) and Cipriani & Pettini (2003), although for rather small systems, detecting a weak decrease of λ_{\max} with increasing N , and by El-Zant (2002) who considered larger N 's and also detected a decreasing Lyapunov exponent when

increasing N .

More recently, Sylos Labini et al. (2015), Benhaïem et al. (2018) and Genel et al. (2018) studied the effect of finite N fluctuations on the properties of the end states of dissipationless cosmological simulations (see also Roy & Perez 2004; Joyce & Marcos 2007a,b; Sellwood & Debattista 2009) finding that, for analogous initial conditions, the particle number N influences both the spurious collisional effects, and the onset of collective instabilities, associated to the long-range nature of the Newtonian force⁴.

In this paper we revisit the problem of finite N -body chaos in equilibrium models of self-gravitating systems, considering the dynamics in the full $2N$ -dimensional phase space as well as individual tracer particle orbits in self-consistent simulations and frozen N -body models. The rest of the paper is structured as follows: in Section 2 we introduce the models and the tools to set the stage for the numerical simulations whose results are presented and discussed in Section 3; in Section 4 we summarize our findings.

2 MODELS AND METHODS

2.1 Initial conditions

We have performed two types of numerical simulations: self-consistent N -body simulations of *equilibrium* spherical systems and single particle orbit integrations in frozen N -body potentials, for various numbers of particles N . In both frozen and self-consistent models, the initial particle positions $\mathbf{r}_{i,0}$ are sampled from two different spherically symmetric density profiles, the flat cored Plummer (1911) profile

$$\rho(r) = \frac{3Mr_c^2}{4\pi(r^2 + r_c^2)^{5/2}}; \quad (3)$$

and the cuspy Hernquist (1990) profile

$$\rho(r) = \frac{M}{2\pi r_c^2 r(1 + r/r_c)^3}, \quad (4)$$

where r_c is a length scale. In the continuum limit, the smooth potentials $\Phi(r)$ generated by the distributions (3) and (4) are central and integrable, thus admitting only regular orbits with $\lambda_{\max} = 0$. For the equilibrium self-consistent models, in order to generate the velocities, we use the standard rejection technique to sample the modulus of the initial velocities $v_{i,0}$ from the isotropic equilibrium phase-space distribution function $f(\mathcal{E})$, with single particle energy per unit mass $\mathcal{E} = v^2/2 + \Phi(r)$, obtained from ρ by means of the Eddington (1916) inversion of Eqs. (1) as

$$f(\mathcal{E}) = \frac{1}{\sqrt{8\pi^2}} \frac{d}{d\mathcal{E}} \int_{\mathcal{E}}^0 \frac{d\rho}{d\Phi} \frac{d\Phi}{\sqrt{\Phi - \mathcal{E}}}. \quad (5)$$

The direction of the velocity vectors is then assigned randomly by sampling a homogeneous distribution in the angular variables (ϑ, φ) and converting the result to Cartesian coordinates.

² The softening of the interactions at small distance might help in making the systems “less collisional”: see Sec. 2.2 below.

³ Note that, due to the long-range nature of the interaction and the fact that in numerical simulations the total energy is rescaled to a constant, all trends with N are valid also with the specific energy E/N if total energy E is not rescaled.

⁴ Remarkably, even in the context of non-neutral plasmas finite- N effects are observed in the asymptotic energy distribution of expanding spherical and ellipsoidal ion bunches, with respect to its continuum limit counterparts (Grech et al. 2011; Saalman et al. 2013; Di Cintio 2014; Zerbe et al. 2018)

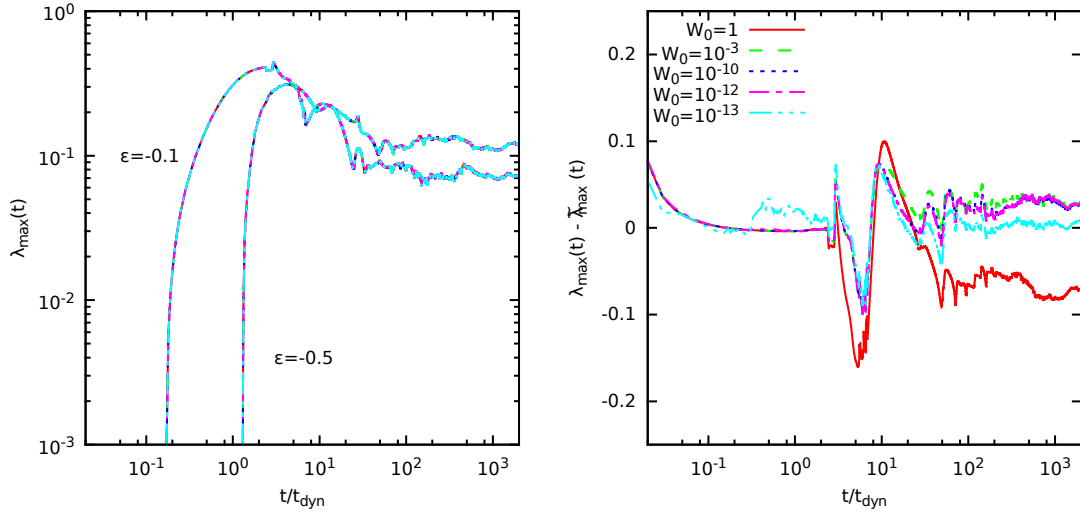


Figure 1. Left panel: Evolution of $\lambda_{\max}(t)$ for two orbits with $\mathcal{E} = -0.1$ and -0.5 evolved in a frozen Plummer potential generated by $N = 10^5$ particles for different initial normalizations of the tangent dynamics \mathbf{W}_6 . Right panel: Evolution of the difference $\lambda_{\max}(t) - \tilde{\lambda}_{\max}(t)$ for the case with $\mathcal{E} = -0.1$ and same choices of the initial normalization.

2.2 Numerical methods and tests

We use an adaptive order symplectic integrator (Kinoshita et al. 1991; Casetti 1995) with fixed time-step Δt to solve the equations of motion

$$\ddot{\mathbf{r}}_i = -Gm \sum_{j=1}^N \frac{\mathbf{r}_i - \mathbf{r}_j}{\|\mathbf{r}_i - \mathbf{r}_j\|^3}, \quad (6)$$

and their associated variational equations for the tangent vectors \mathbf{w}_i (Miller 1971; Goodman et al. 1993; Hemsendorf & Merritt 2002; Rein & Tamayo 2016)

$$\ddot{\mathbf{w}}_i = -Gm \sum_{j=1}^N \left[\frac{\mathbf{w}_i - \mathbf{w}_j}{\|\mathbf{r}_i - \mathbf{r}_j\|^3} - 3(\mathbf{r}_i - \mathbf{r}_j) \frac{(\mathbf{w}_i - \mathbf{w}_j) \cdot (\mathbf{r}_i - \mathbf{r}_j)}{\|\mathbf{r}_i - \mathbf{r}_j\|^5} \right] \quad (7)$$

that are needed to compute the Lyapunov exponent (see below). As a rule, we use the 4th order integrator with $\Delta t = 10^{-2} t_{\text{dyn}}$ for models with $N < 3 \times 10^4$ and the 2nd order integrator with $\Delta t = 3.3 \times 10^{-3} t_{\text{dyn}}$ for larger system sizes. Throughout this work we assume units such that $G = M = r_c = 1$, so that the dynamical time is given by $t_{\text{dyn}} = \sqrt{r_c^3/GM}$ and the scale velocity $v_{\text{typ}} = r_c/t_{\text{dyn}}$ also equal 1. Individual particle masses are then $m = 1/N$.

Typically, in direct N -body simulations, the divergence of the Newtonian potential for vanishing interparticle separation, leading to the accumulation of round-off errors in the trajectories, is cured by introducing the softening length ϵ_{soft} so that the potential at distance r from a particle of mass m becomes $\phi(r) = -Gm/\sqrt{r^2 + \epsilon_{\text{soft}}^2}$. For our choice of timestep Δt we take as optimal value of the softening $\epsilon_{\text{soft}} = 5 \times 10^{-3} r_c$ (for a detailed analysis of the relation between the optimal values of Δt and ϵ_{soft} , see Dehnen & Read 2011, and references therein). We verified that, at fixed ϵ_{soft} , the results of the numerical simulations are unchanged when anteriorly decreasing Δt . Tracer particle integrations in frozen potentials are extended up to $t = 2000 t_{\text{dyn}}$, while self-consistent equilibrium N -body simulations to $t = 200 t_{\text{dyn}}$, for all the values of N . It is worth noting that the softening

of the interactions not only cures the numerical problems related to the divergence of the $1/r$ potential when $r \rightarrow 0$, but also makes the system “less collisional” than a system with the same N particles but unsoftened interactions, because the strongest collisions where particles become really close to each other have a much smaller impact on the system. However, the two-body relaxation time still grows with N as $\ln N$ (see e.g. Gabrielli et al. 2010).

As mentioned above, a quantitative measure of the degree of chaotic instability of the dynamics is given by the largest Lyapunov exponent, measuring the exponential growth rate of perturbations of a given trajectory in phase space. We compute the numerical estimate of the largest Lyapunov exponent by means of the standard Benettin et al. (1976) method (see also Contopoulos 2002; Ginelli et al. 2007, 2013) as

$$\lambda_{\max}(t) = \frac{1}{L\Delta t} \sum_{k=1}^L \ln \frac{W(k\Delta t)}{W_0}, \quad (8)$$

for a (large) time $t = L\Delta t$, where W is the norm of the $6N$ -dimensional vector

$$\mathbf{W}_{6N} = (\mathbf{w}_i, \dot{\mathbf{w}}_i, \dots, \mathbf{w}_N, \dot{\mathbf{w}}_N), \quad (9)$$

for self-consistent simulations, and of the six-dimensional vector

$$\mathbf{W}_6 = (\mathbf{w}, \dot{\mathbf{w}}), \quad (10)$$

for a tracer in a frozen N -body model. In both cases, W_0 is the value of such norm at $t = 0$. The “true” largest Lyapunov exponent would correspond to the limit for $L \rightarrow \infty$ in Eq. (8), therefore what we compute is, properly speaking, the finite-time Lyapunov exponent $\lambda_{\max}(t)$, that may differ from the true asymptotic value $\lambda_{\max} = \lim_{t \rightarrow \infty} \lambda_{\max}(t)$. However, we checked that L is large enough for the result to appear relaxed to its asymptotic value, so that we may be confident that our long-time results are a good approximation to λ_{\max} . Hereafter, to avoid confusion, we will use λ_{\max} to denote the largest Lyapunov exponent of a single particle orbit in a frozen potential, and Λ_{\max} for the largest Lyapunov ex-

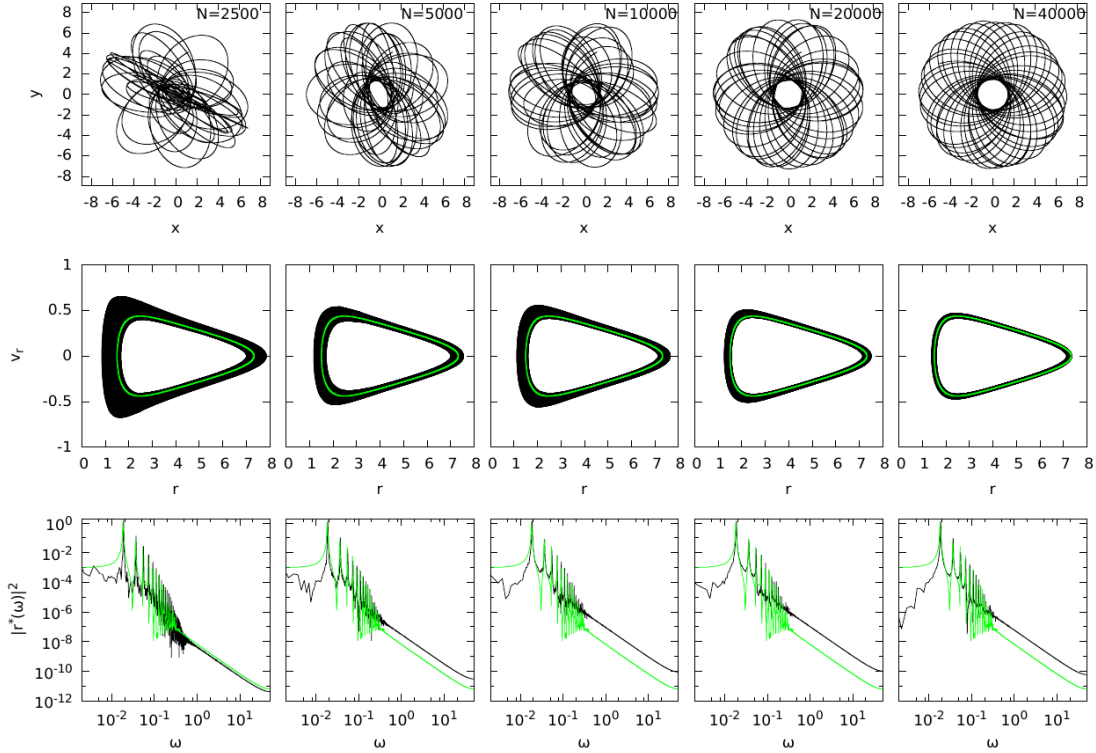


Figure 2. Top row: projections on the x, y plane of five tracer orbits starting with the same initial condition $(\mathbf{r}_0, \mathbf{v}_0)$, with energy per unit mass $\mathcal{E} = -0.1$, evolved in a frozen N -body potential generated by a discrete Plummer distribution of $N = 2.5 \times 10^3, 5 \times 10^3, 10^4, 2 \times 10^4$ and 4×10^4 particles. Middle row: orbit section in the r, v_r plane. Bottom row: squared modulus of the Fourier spectrum of the radial coordinate r . In all plots the black lines refer to the discrete models, while the green (gray) ones to the same initial condition propagated in the parent smooth potential.

ponent of the full $6N$ -dimensional self consistent problem. To improve convergence, following Benettin et al. (1976), the vector $\mathbf{W}_{6N,6}$ is periodically renormalized to W_0 . In all simulations presented here, the renormalization procedure is done every $10\Delta t$. The final value attained by λ_{\max} (or Λ_{\max}) is independent on the frequency of this operation and the value of W_0 , that we fix to unity in all simulations shown here.

We note that in previous works several authors (see e.g. Sideris 2004; Kandrup et al. 2004; Meschiari 2006) used, in order to evaluate Eq. (8) for a tracer particle, the difference between two realizations of the same orbit starting with initial conditions $(\mathbf{r}_0, \mathbf{v}_0)$ and $(\mathbf{r}'_0, \mathbf{v}'_0)$, i.e. $\tilde{\mathbf{W}}_6 = (\mathbf{r} - \mathbf{r}', \mathbf{v} - \mathbf{v}')$ instead of the tangent vectors. By doing so, the value of the largest Lyapunov exponent $\tilde{\lambda}_{\max}$ strongly depends on the choice of \tilde{W}_0 , at variance with its counterpart evaluated using the tangent dynamics that, in general, has a different value independent on W_0 . In order to assess the magnitude of such discrepancy, we have performed some test simulations where two realizations of a given trajectory with different initial distance \tilde{W}_0 in the range $(10^{-13}, 1)$ were integrated in the frozen potential generated by a distribution of N particles extracted from a Plummer distribution, for various N . We computed the largest Lyapunov exponent over $2000 t_{\text{dyn}}$ by means of the standard expression (8) using the tangent vectors, as well as using the difference between the two realizations, having set in all cases $\mathbf{W}_6 = \tilde{\mathbf{W}}_6$ at $t = 0$. We observed that, as

expected, the values attained by the Lyapunov exponent computed in the “correct” way is independent on the initial value of the norm for all orbit energies and system sizes, as shown in the left panel of Fig. (1) for two particles with initial energies $\mathcal{E} = -0.1$ and -0.5 in a frozen Plummer model with $N = 10^5$. On the contrary, when evaluating $\tilde{\lambda}_{\max}$ using the difference between two initially close realizations of the same orbit, its value is significantly different from $\lambda_{\max}(t)$ at all times for $\tilde{W}_0 > 10^{-13}$. This is exemplified in the right panel of Fig. (1), where $\lambda_{\max}(t) - \tilde{\lambda}_{\max}(t)$ is plotted as function of time, and it can be clearly seen to converge to zero only for the smallest choice of \tilde{W}_0 . We finally mention that the rôle played by softening in affecting chaos in self-gravitating systems has been studied by Komatsu et al. (2009).

3 SIMULATIONS AND RESULTS

3.1 Orbits in frozen N -body potentials

Single particle orbits in frozen N -body self-gravitating systems have been extensively used to study the dynamics in triaxial systems for which analytic formulations of the phase-space distribution function are unknown (see e.g. Kandrup et al. 2004; Contopoulos & Harsoula 2013; Manos & Machado 2014; Machado & Manos 2016; Chaves-Velasquez et al. 2017; Patsis & Harsoula 2018, and references therein) and are usually constructed numerically using orbit libraries

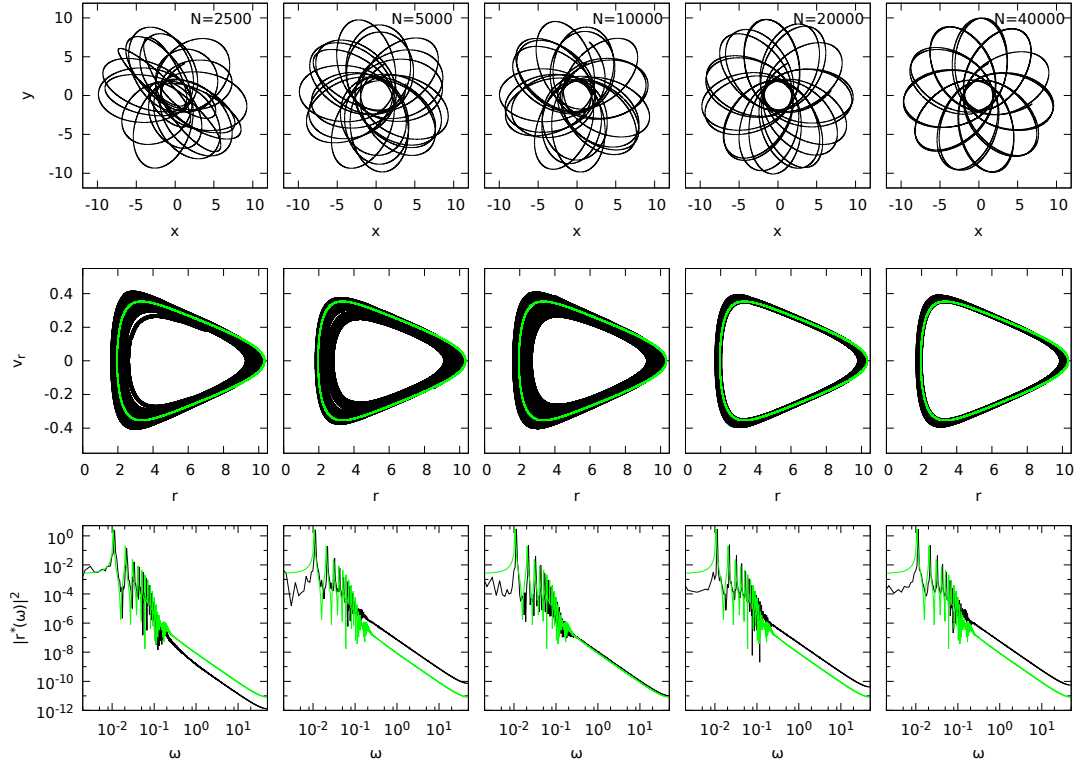


Figure 3. Same as in Fig. 3 but for a Hernquist model.

(Schwarzschild 1979; Terzić 2002, 2003). It is well known (see e.g. Merritt & Valluri 1996, 1998; Valluri & Merritt 1998) that triaxial potentials are associated to mixed phase-space, admitting regions with both regular and chaotic orbits. When it comes to the study of discrete N -body models, it is not always easy to determine on which extent the chaos is due to the discreteness or to the finite deviation from spherical symmetry.

In this paper we study the orbital structure and the scaling of the the largest Lyapunov exponent as a function of the number of particles N in *spherical* models, starting with their frozen realizations. We have evolved the same initial condition $(\mathbf{r}_0, \dot{\mathbf{r}}_0)$ in the frozen N -body realizations of Plummer and Hernquist density profiles for $10^2 \leq N \leq 3 \times 10^7$. In Figs. 2-3 we show, for Plummer and Hernquist models, respectively, the same initial conditions propagated in the potential of a frozen N -body model for $N = 2.5 \times 10^3, 5 \times 10^3, 10^4, 2 \times 10^4$ and 4×10^4 . For both models, as N increases the orbit projection in the x, y plane (upper rows) becomes more and more regular and markedly centrophobic (cfr. analogous plots in Kandrup & Sideris 2001; Sideris & Kandrup 2002; Kandrup et al. 2004). Consistently, and as expected, the radial phase-space sections r, v_r (middle rows) show that the orbit propagated in the discrete frozen potential (black dots) approaches that in the smooth potential (green/gray dots) for increasing values of N . As a general trend, and for both choices of $\rho(r)$ the phase-space sections show a larger diffusion from the “analytic orbit” at low radii and are bound between two limit curves up to $t = 2 \times 10^3 t_{\text{dyn}}$ (the time to which the frozen N -body integrations are extended). On

the other hand, the behaviour of Fourier spectra of the radial coordinate r , $|r^*(\omega)|^2$ (bottom rows) has a less trivial trend with the system size N . For both Plummer and Hernquist density profiles, the peak in the spectrum corresponding to the fundamental radial frequency ω_r does not appear to be significantly shifted with respect to that of the orbit in the smooth potential. The low and high frequency tails do not appear to have any significant trend with N for the Plummer model, while appear to reproduce better the spectrum of the orbit integrated in the smooth potential for intermediate N (e.g. $N = 10^4$ in Fig. 3). We found that such effect on the orbits in Fourier space does not depend either on the orbit energy (per unit mass) \mathcal{E} nor on the magnitude of the initial angular momentum J . In Figure 4, as an example, we show $|r^*(\omega)|^2$ for three different initial conditions evolved in a frozen Plummer model. In all cases the orbits have comparable values of energy per unit mass, while the initial angular momentum⁵ \mathbf{J}_0 has significantly different values in the three rows of curves. It is apparent that for tracer orbits starting with vanishing initial angular momentum (upper row), and the maximum attainable angular momentum (bottom row), increasing the value of N has little effect on improving the matching between the discrete Fourier spectra with that of the orbit in the smooth potential.

For both frozen Plummer and Hernquist models we have evaluated the maximal Lyapunov exponent λ_{max} for orbits

⁵ Note that \mathbf{J} is conserved only for orbits propagated in the smooth potential.

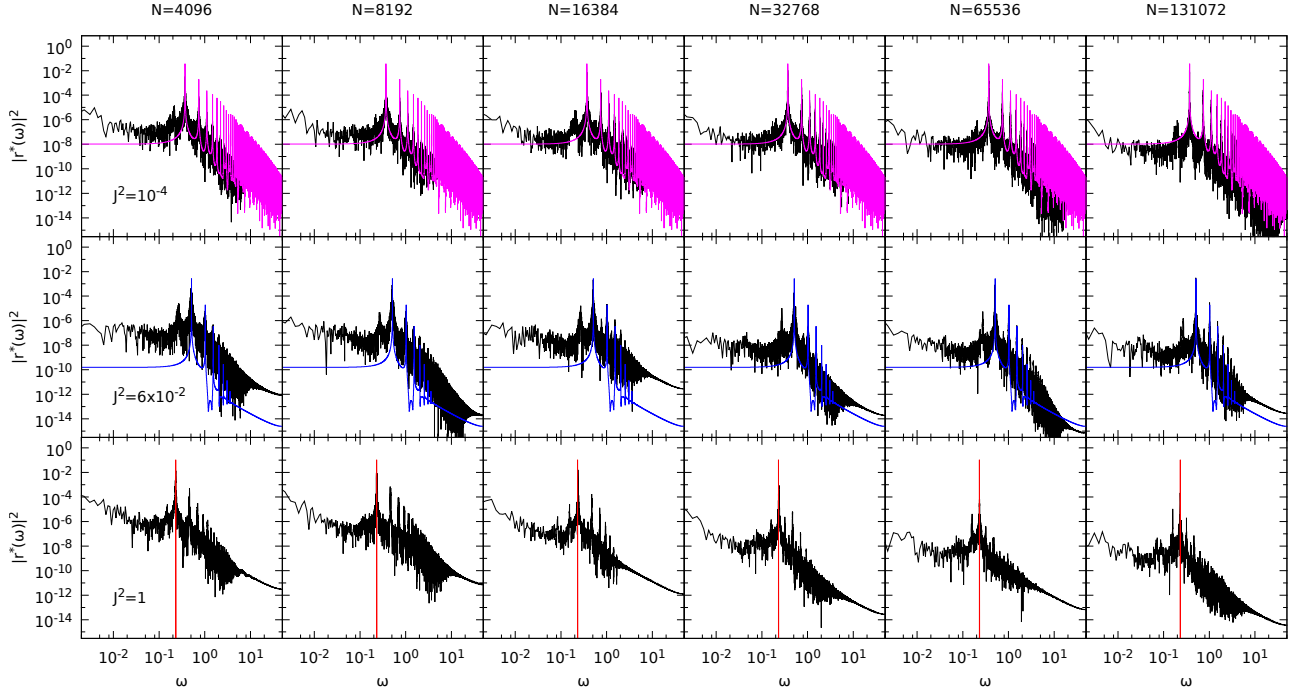


Figure 4. Fourier spectra of radial coordinates of orbits with $\mathcal{E} = -0.8$ propagated in a frozen Plummer model with increasing N and different values of angular momentum $J^2 = 10^{-4}$ (upper panels), 6×10^{-2} (middle panels), and 1 (bottom panels). The black curves refer to the orbit in the frozen N -body potential, while the coloured (gray) ones to the corresponding orbit propagated in the smooth Plummer potential.

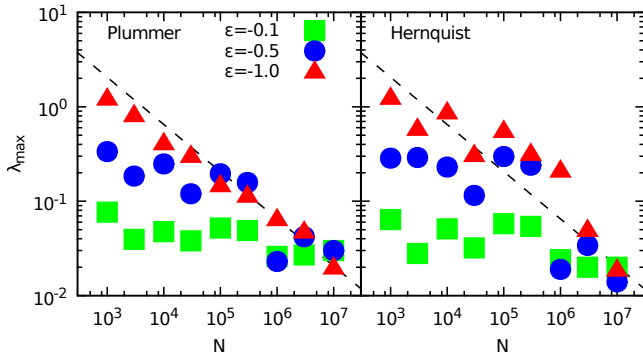


Figure 5. Largest Lyapunov exponent λ_{\max} for a tracer orbit with $\mathcal{E} = -0.1, -0.5$ and -1 in a frozen N -body model as a function of N , for Plummer (left panel) and Hernquist (right panel) profiles. The dashed line is the $N^{-1/2}$ law.

with different values of the energy per unit mass \mathcal{E} . Figure 5 illustrates the trend of λ_{\max} for three typical orbital energy values $\mathcal{E} = -0.1, -0.5, -1$. The value of the Lyapunov exponent seems to be almost independent of the number of particles N for weakly bound orbit (i.e., $\mathcal{E} = -0.1$ in this case), while it seems to approach a $\lambda \propto N^{-1/2}$ trend as the tracer orbit is more and more bound.

3.2 Self-consistent equilibrium models

We repeated the above described analysis for active particles with the same initial conditions $(\mathbf{r}_0, \mathbf{v}_0)$ in self-consistent N -body runs with the same values of N (see Figs. 6, 7). From the point of view of the orbital structure, for both Plummer and Hernquist models, the situation in this case is more consistent with what one would expect, with more similar spectra at larger N . In particular, as N increases individual particle orbits become more regular (even though less rapidly than in frozen N -body models) and explore less and less phase-space.

Additionally, we have computed the maximal Lyapunov exponent λ_{\max}^* for a tracer particle moving in an active self-consistent model for both choices of the density profile and different values of its energy per unit mass \mathcal{E} . Surprisingly, λ_{\max}^* shows little dependence on N for active systems and rapidly converges to *lower* values than its counterpart for frozen systems even though individual orbits in configuration space appear to be less regular as shown in Fig. 8. Moreover, the value of λ_{\max}^* for tracer particles in self-consistent systems is also strongly dependent on its initial energy \mathcal{E}_0 , with more bound particles having more chaotic orbits associated with larger λ_{\max}^* at larger N .

We interpret these facts as a hints that the continuum limit shall be questioned at least concerning the concept of N -body chaos. In particular, the diffusion in phase-space (connected to relaxation phenomena such as violent relax-

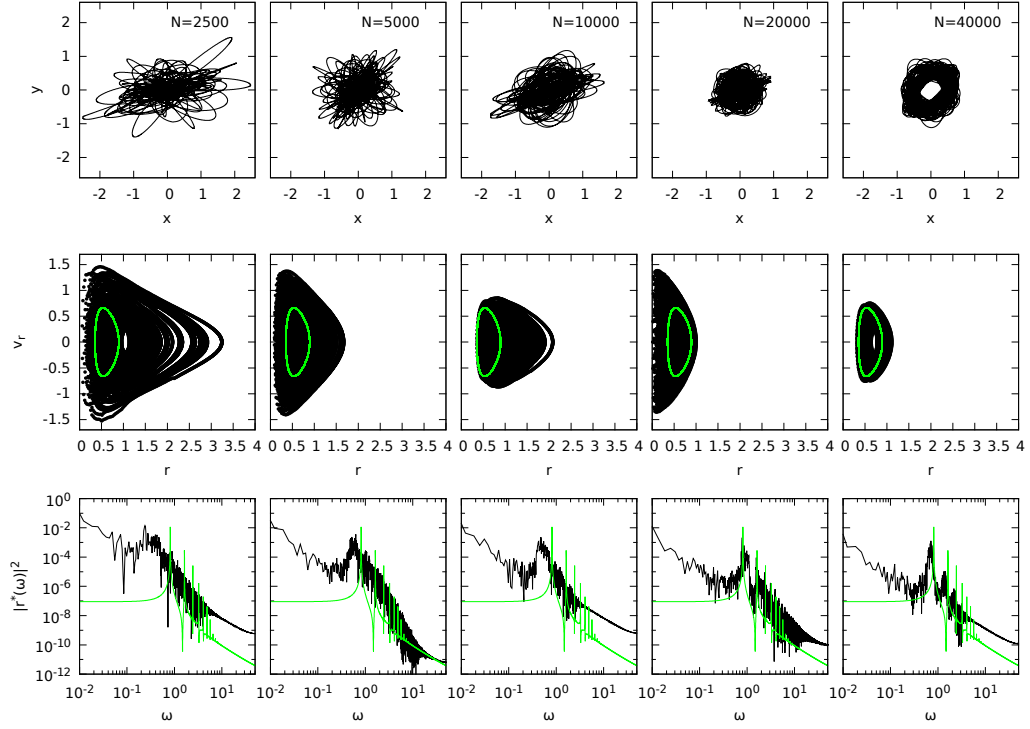


Figure 6. Top row: projections on the (x, y) plane of five tracer orbits starting with the same initial condition $(\mathbf{r}_0, \mathbf{v}_0)$, again with initial energy per unit mass $\mathcal{E} = -0.1$ in a self-consistent N -body simulation with initial conditions sampled from an isotropic Plummer model with $N = 2.5 \times 10^3, 5 \times 10^3, \times 10^4, 2 \times 10^4$ and 4×10^4 particles. Middle row: orbit section in the r, v_r plane. Bottom row: squared modulus of the Fourier spectrum of the radial coordinate r .

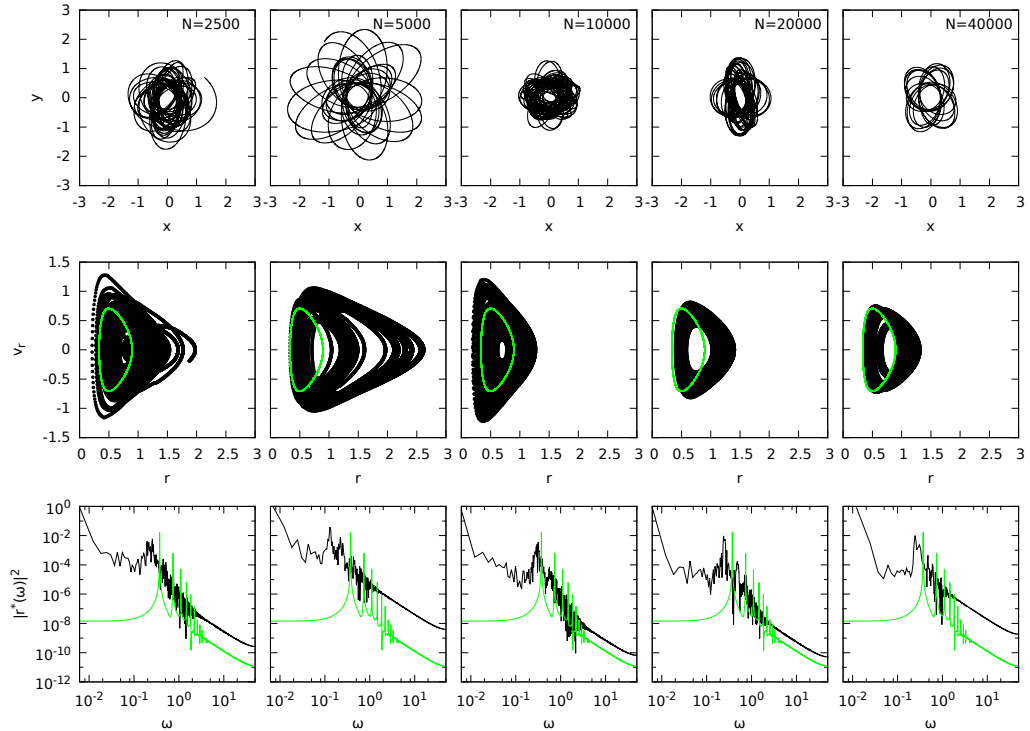


Figure 7. The same as in Fig. 7 for a Hernquist model.

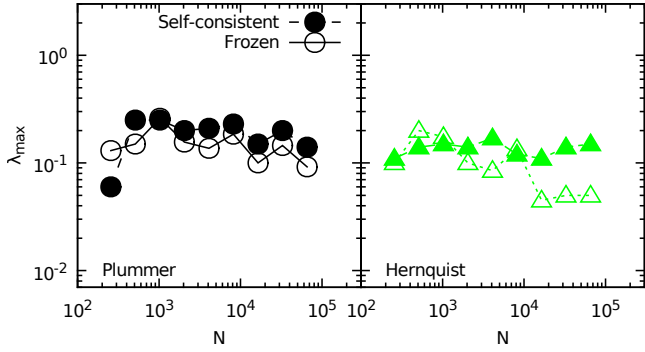


Figure 8. Largest Lyapunov exponent λ_{\max}^* for a non-interacting tracer particle in an isotropic self-consistent N -body model (full symbols) and Largest Lyapunov exponent λ_{\max} for the same particle in a frozen N -body model (empty symbols), as a function of N , for Plummer (left panel) and Hernquist (right panel) density profiles.

ation and phase mixing) should be quite different in the two cases since in a frozen model the single particle energy is always conserved independently of N , while in active N -body models particles could exchange energy, even in the limit $N \rightarrow \infty$. This is exemplified in Fig. 9 where we show at different times ($t = 0, 5, 10$ and $50 t_{\text{dyn}}$) the positions in the (x, y) and (x, v_x) planes of an initially localized bunch of $N_t = 500$ tracers propagated in a $N = 32768$ self consistent Plummer model. Tracer particles rapidly explore a large portion of configuration and phase-space, while they tend to remain localized in the frozen case (data not shown).

From the trend with N of the maximal Lyapunov exponent Λ_{\max} for an active self-consistent model (Fig. 10), it is apparent that the degree of chaoticity of such a system strongly depends on the nature of the density profile, with cuspy models being in general more chaotic for large N . In both cases the largest Lyapunov exponent decreases with N ; for the N 's explored here, the values of the Lyapunov time (that is, Λ_{\max}^{-1}) remain within one order of magnitude around the dynamical time. In the Plummer case the dependence on N is well described by a $N^{-1/2}$ law, while in the Hernquist case the N -dependence is weaker and, although the values are consistently decreasing up to $N \approx 10^5$, a saturation for large values of N can not be totally ruled out by our results. We note that our results for Λ_{\max} are given in units of t_{dyn}^{-1} , that, as mentioned above, is always equal to unity. Cipriani & Pettini (2003) introduced a dimensionless maximal Lyapunov exponent or “dimensionless chaoticity indicator” as $\gamma_1 \equiv \Lambda_{\max} t_{\text{dyn}}$. Such quantity, at variance with Λ_{\max} computed here, was found to be independent of N and on the average particle energy. Note that, however, the value of $t_{\text{dyn}} = \sqrt{G\rho}$ used by Cipriani & Pettini (2003) depends on the mass density ρ that we keep fixed, while in their case varies as a function of N , thus restoring a dependence on the number of particles of the dynamical time.

4 SUMMARY AND CONCLUSIONS

We have investigated the chaotic properties of the dynamics of N -body self-gravitating systems, studying single-particle orbits in frozen and active potentials as well as the dynamics

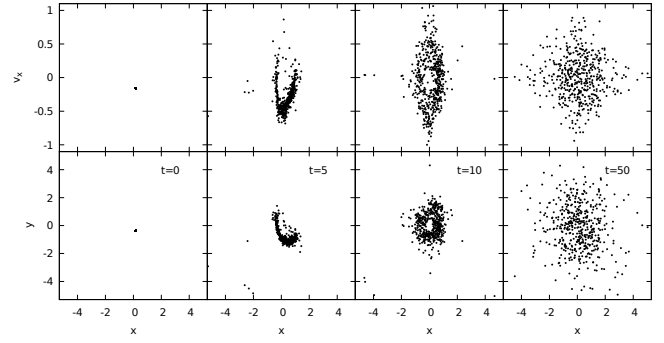


Figure 9. Evolution of a distribution of $N_t = 500$ non-interacting tracers in a self consistent Plummer model with $N = 32768$.

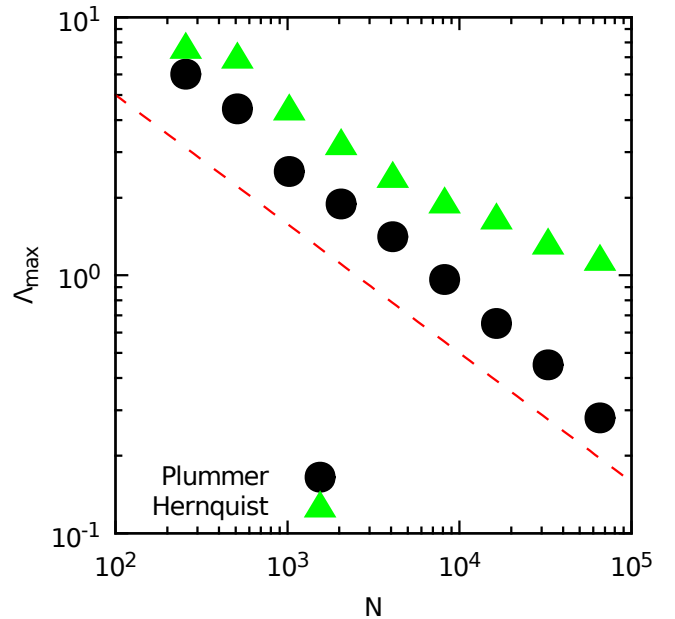


Figure 10. Largest Lyapunov exponent Λ_{\max} for an isotropic self-consistent N -body model as function of N , for Plummer (circles) and Hernquist (triangles) profiles. The dashed line is the $N^{-1/2}$ law.

in the full $2N$ -dimensional phase space. Initial conditions were always drawn from spherically symmetric stationary models, namely, the flat-cored Plummer model and the centrally cuspy Hernquist model.

The main results of this study can be summarized as follows. As to the properties of single-particle orbits, the orbital structure of particles in frozen N -body models approaches that of continuum potentials, however the dependence on N of this trend is not trivial. Moreover, orbits in frozen models and active self-consistent models have (obviously) different mixing properties and have, in general, different largest Lyapunov exponents; the dependence of the largest Lyapunov exponent on N is more pronounced in frozen systems than in active ones.

Given that orbits in potentials that are integrable in the continuum limit behave differently in frozen and self-consistent simulations, we argue that nothing can be safely deduced from studies with tracer particles in frozen N -body

models reproducing non-integrable models, such as, for example, triaxial systems.

As far as the chaotic properties of the dynamics in the full $2N$ -dimensional phase space is concerned, our results confirm the expectation (and previous results, at least qualitatively; see e.g. El-Zant 2002) that systems with larger N are less chaotic. However, the actual value of the largest Lyapunov exponent as well as its dependence on N depend on the chosen equilibrium model: the flat-cored Plummer model has smaller Lyapunov exponents that are proportional to $N^{-1/2}$, while the Lyapunov exponents of the cuspy Hernquist model are systematically larger than the Plummer ones and their dependence on N is considerably weaker.

This established, it remains to clarify whether the present results could be extended to axisymmetric and triaxial models (admitting in the continuum limit the coexistence of regions of regular and chaotic dynamics), or spherical models with velocity anisotropy. The interplay between N -body chaos and external noise in models characterized by Osipkov-Merritt radial anisotropy will be explored in a forthcoming publication.

ACKNOWLEDGMENTS

We thank Matteo Sala and Francesco Ginelli for insightful discussions and relevant comments at an early stage of this work. One of us (PFDC) wishes to thank Christos Efthymiopoulos and the hospitality of the Center for Astronomy and Applied Mathematics of the Academy of Athens where part of this work was completed.

References

Antoni M., Ruffo S., 1995, *Phys. Rev. E*, 52, 2361
 Benettin G., Galgani L., Strelcyn J.-M., 1976, *Phys. Rev. A*, 14, 2338
 Benhaïem D., Joyce M., Sylos Labini F., Worrakitpoonpon T., 2018, *MNRAS*, 473, 2348
 Binney J., Tremaine S., 2008, *Galactic Dynamics: Second Edition*. Princeton University Press
 Campa A., Dauxois T., Ruffo S., 2009, *Physics Reports*, 480, 57
 Campa A., Dauxois T., Fanelli D., Ruffo S., 2014, *Physics of Long-Range Interacting Systems*. Oxford University Press, Oxford
 Casetti L., 1995, *Phys. Scr.*, 51, 29
 Cerruti-Sola M., Pettini M., 1995, *Phys. Rev. E*, 51, 53
 Chandrasekhar I. S., 1941, *ApJ*, 93, 285
 Chaves-Velasquez L., Patsis P. A., Puerari I., Skokos C., Manos T., 2017, *ApJ*, 850, 145
 Cipriani P., Pettini M., 2003, *Ap&SS*, 283, 347
 Contopoulos G., 2002, *Order and chaos in dynamical astronomy*
 Contopoulos G., Harsoula M., 2013, *MNRAS*, 436, 1201
 Dehnen W., Read J. I., 2011, *European Physical Journal Plus*, 126, 55
 Di Cintio P., 2014, PhD thesis, Technische Universität Dresden ([arXiv:1408.3857](https://arxiv.org/abs/1408.3857))
 Eddington A. S., 1916, *MNRAS*, 76, 572
 El-Zant A. A., 2002, *MNRAS*, 331, 23
 El-Zant A., Everitt M., Kassem S., 2018, preprint, ([arXiv:1804.06920](https://arxiv.org/abs/1804.06920))
 Filho L. H. M., Amato M. A., Rocha Filho T. M., 2018, *Journal of Statistical Mechanics: Theory and Experiment*, 3, 033204
 Gabrielli A., Joyce M., Marcos B., 2010, *Physical Review Letters*, 105, 210602

Genel S., et al., 2018, preprint, ([arXiv:1807.07084](https://arxiv.org/abs/1807.07084))
 Ginelli F., Poggi P., Turchi A., Chaté H., Livi R., Politi A., 2007, *Physical Review Letters*, 99, 130601
 Ginelli F., Takeuchi K. A., Chaté H., Politi A., Torcini A., 2011, *Phys. Rev. E*, 84, 066211
 Ginelli F., Chaté H., Livi R., Politi A., 2013, *Journal of Physics A Mathematical General*, 46, 254005
 Goodman J., Heggie D. C., Hut P., 1993, *ApJ*, 415, 715
 Grech M., et al., 2011, *Phys. Rev. E*, 84, 056404
 Helmi A., Gomez F., 2007, preprint, ([arXiv:0710.0514](https://arxiv.org/abs/0710.0514))
 Hemsendorf M., Merritt D., 2002, *ApJ*, 580, 606
 Hernquist L., 1990, *ApJ*, 356, 359
 Joyce M., Marcos B., 2007a, *Phys. Rev. D*, 75, 063516
 Joyce M., Marcos B., 2007b, *Phys. Rev. D*, 76, 103505
 Kandrup H. E., 1998a, *ApJ*, 500, 120
 Kandrup H. E., 1998b, *Annals of the New York Academy of Sciences*, 848, 28
 Kandrup H. E., 2001, *MNRAS*, 323, 681
 Kandrup H. E., Novotny S. J., 2004, *Celestial Mechanics and Dynamical Astronomy*, 88, 1
 Kandrup H. E., Sideris I. V., 2001, *Phys. Rev. E*, 64, 056209
 Kandrup H. E., Sideris I. V., 2003, *ApJ*, 585, 244
 Kandrup H. E., Siopis C., 2003, *MNRAS*, 345, 727
 Kandrup H. E., Vass I. M., Sideris I. V., 2003, *MNRAS*, 341, 927
 Kandrup H. E., Sideris I. V., Bohn C. L., 2004, *Physical Review Special Topics Accelerators and Beams*, 7, 014202
 Kinoshita H., Yoshida H., Nakai H., 1991, *Celestial Mechanics and Dynamical Astronomy*, 50, 59
 Komatsu N., Kiyata T., Kimura S., 2009, *Physica A Statistical Mechanics and its Applications*, 388, 639
 Lichtenberg A., Lieberman M., 1992, *Regular and Chaotic Dynamics*
 Machado R. E. G., Manos T., 2016, *MNRAS*, 458, 3578
 Manos T., Machado R. E. G., 2014, *MNRAS*, 438, 2201
 Manos T., Ruffo S., 2011, *Transport Theory and Statistical Physics*, 40, 360
 Merritt D., Valluri M., 1996, *ApJ*, 471, 82
 Merritt D., Valluri M., 1998, *Annals of the New York Academy of Sciences*, 858, 48
 Meschiari S., 2006, Master's thesis, Bologna University
 Miller R. H., 1964, *ApJ*, 140, 250
 Miller R. H., 1971, *Journal of Computational Physics*, 8, 449
 Monechi B., Casetti L., 2012, *Phys. Rev. E*, 86, 041136
 Patsis P. A., Harsoula M., 2018, *A&A*, 612, A114
 Plummer H. C., 1911, *MNRAS*, 71, 460
 Rein H., Tamayo D., 2016, *MNRAS*, 459, 2275
 Roy F., Perez J., 2004, *MNRAS*, 348, 62
 Saalmann U., Mikaberidze A., Rost J. M., 2013, *Physical Review Letters*, 110, 133401
 Schwarzschild M., 1979, *ApJ*, 232, 236
 Sellwood J. A., Debattista V. P., 2009, *MNRAS*, 398, 1279
 Sideris I. V., 2002, PhD thesis, UNIVERSITY OF FLORIDA
 Sideris I. V., 2004, *Celestial Mechanics and Dynamical Astronomy*, 90, 147
 Sideris I. V., Kandrup H. E., 2002, *Phys. Rev. E*, 65, 066203
 Sideris I. V., Kandrup H. E., 2004, *ApJ*, 602, 678
 Sylos Labini F., Benhaïem D., Joyce M., 2015, *MNRAS*, 449, 4458
 Terzić B., 2002, PhD thesis, THE FLORIDA STATE UNIVERSITY
 Terzić B., 2003, *ArXiv Astrophysics e-prints*,
 Terzić B., Kandrup H. E., 2003, *ArXiv Astrophysics e-prints*,
 Tsuchiya T., Gouda N., 2000a, in Gurzadyan V. G., Ruffini R., eds, *The Chaotic Universe*. pp 259–267, doi:10.1142/9789812793621_0016
 Tsuchiya T., Gouda N., 2000b, *Phys. Rev. E*, 61, 948
 Valluri M., Merritt D., 1998, *ApJ*, 506, 686
 Zerbe B. S., Xiang X., Ruan C.-Y., Lund S. M., Duxbury P. M., 2018, *Physical Review Accelerators and Beams*, 21, 064201